Jingxiang Shu[1]*, Asaad Y. Shamseldin[1], Evan Weller[2]

[1]Department of Civil and Environmental Engineering, The University of Auckland, Private Bag 92019, Auckland Mail Centre, Auckland 1142, New Zealand.

[2] School of Environment, The University of Auckland, Private Bag 92019, Auckland Mail Centre, Auckland 1142, New Zealand.

Corresponding author: Jingxiang Shu (jshu987@aucklanduni.ac.nz)

Key Points:

- The spatial variability of AR-induced heavy rainfall is related to AR's orientation and landfall direction in New Zealand
- ARs have a northwesterly landfall direction and orientation are the major contributor to water resources
- A modified AR impact ranking scale was evaluated regarding AR's orientation and landfall direction

Abstract

Atmospheric Rivers (ARs) are filamentary channels of strong poleward water vapour transport in the midlatitudes. Recent studies have found that ARs are northwesterly and northeasterly orientated and can make landfall in all directions over New Zealand. In this study, we further investigate the characteristics, in particular orientation and landfall direction, of detected landfalling ARs based on two atmospheric reanalysis datasets over 35 years. Daily rainfall records from 655 rain gauges between 1979 to 2018 were used to investigate the spatial variability of the AR contribution to annual rainfall and extreme rainfall linked with AR events with different orientations and mean landfall directions. A modified AR impact ranking scale was then evaluated regarding AR-event orientation and mean landfall direction, different "AR impact" sectors, and peak daily AR-event rainfall. We found that landfalling ARs (events) with a northwesterly orientation and northwesterly landfall direction (NW-NW ARs) are the most frequent and relatively stronger, more coherent and concentrated over the country. As a result, NW-NW ARs are major contributors to annual rainfall and extreme rainfall for the country's West Coast. Generally, the windward side experiences anomalously high rainfall as ARs reach the country from different directions, and the spatial distribution of AR-event heavy rainfall is shown to vary with an AR's orientation and landfall direction. Moreover, the AR impact ranking scale performs well for NW-NW ARs over the West Coast. However, more factors need to be considered to improve the applicability of the scale on the East Coast.

1 Introduction

Atmospheric rivers (ARs) are filamentary channels of enhanced poleward water vapour transport in the lower troposphere, primarily occurring in the midlatitudes (Newell et al., 1992; Newell & Zhu, 1994; Ralph et al., 2004, 2005, 2018;

Zhu & Newell, 1994, 1998). Furthermore, ARs are an important component of the global water cycle, and their presence is often tied with frontal (Liu et al., 2021; Ralph et al., 2004, 2005; Zhu & Newell, 1998) and cyclone (Cordeira et al., 2013; Guo et al., 2020; Ralph et al., 2004, 2005; Sodemann & Stohl, 2013; Zhang et al., 2019; Zhou & Kim, 2019; Zhu & Newell, 1994) features. AR-induced extreme precipitation usually occurs on the windward side of mountainous coastal regions (Blamey et al., 2018; Lamjiri et al., 2017; Lavers & Villarini, 2013a; Neiman et al., 2011; Ralph & Dettinger, 2012; Ralph et al., 2006; Viale et al., 2018). Depending on the soil condition and season, these AR-related extreme rainfall events can further cause floods (Dettinger et al., 2011; Lavers et al., 2011, 2012; Neiman et al., 2011; Ralph et al., 2013; Ralph et al., 2006) and/or mitigate droughts (de Kock et al., 2021; Dettinger, 2013). Additionally, many inland floods and extreme precipitation are associated with an AR's inland penetration (Lavers & Villarini, 2013a, 2013b; Nayak & Villarini, 2017). On the other hand, ARs are major contributors to water resources where they frequently occur (Dettinger et al., 2011; Lavers & Villarini, 2015; Nayak & Villarini, 2017; Viale et al., 2018). Globally, extreme precipitation and damaging wind events are related to ARs (Waliser & Guan, 2017). The occurrence of droughts and floods are likely to be caused by the absence and presence of ARs, respectively (Paltan et al., 2017).

Despite the orographic control on a landfalling AR's impact, AR origin and landfall direction can affect the precipitation amount on landfall locations. By tracking the AR objects spatiotemporally, Zhou and Kim (2019) distinguished winter (DJF) landfalling ARs by their origins over the U.S. West Coast (30°N-49°N). They found that the characteristics and the impact on precipitation of landfalling AR events from the Northwest Pacific (WLAR) (20°N-45°N, 120°E-170°W) and Northeast Pacific (ELAR) (20°N-45°N, 125°W-170°W) vary notably. For example, WLAR events generally have longer lifetimes and stronger intensities than ELAR events. Daily precipitation from WLAR events persists between 40°N and 60°N. In contrast, ELAR events see precipitation more between 35°N and 45°N. This difference is because ARs originate from different locations tend to make landfall on different areas (Zhou and Kim, 2019). In addition, AR-induced precipitation patterns can vary remarkably due to different landfall AR directions within different synoptic-scale flow regimes. For example, Hecht and Cordeira (2017) found that more heavy precipitation is associated with south-southwesterly ARs than westerly ARs over the Russian River Watershed due to the more favourable landfall direction against the local topography orientation and stronger ARs.

New Zealand is a long and narrow country surrounded by ocean and spanning from 34°S to 47°S in the midlatitudes. Mountain ranges in the country trend southwest-northeast peaking at 3764 m. Compared to the U.S. West Coast region, the AR-precipitation mechanism may well be different owing to the country's geographical location and landmass. Main precipitation-generating weather systems are cyclones in the Tasman Sea and tropical cyclones from the north passing or near northern regions of the country, and fronts and depres-

sions within the band of westerlies to the south of the country (Salinger, 1980). In combination with orographic uplift, there are four main rainfall mechanisms common throughout the country: uplift within cold fronts and cyclones embedded in the westerlies; enhanced rainfall on the windward side of mountain ranges due to orographic uplift; convective rainfall due to summer heating in eastern regions; subtropical frontal systems from the north (Tait & Fitzharris, 1998). Overall, anomalously high precipitation tends to distribute along the windward side of most coastal areas than the leeward side due to the orographic uplift on the windward air streams along most coastlines (Salinger, 1980). For example, anomalously high precipitation events can occur on the east coast of the South Island of the country when a quasi-stationary depression occurs in the Tasman Sea, to the west of the North Island, with westerly anticyclones moving to the South Island (Salinger, 1980). It is noteworthy that localised heavy precipitation can occur as the unstable windward air advection takes place even for relatively flat areas such as the Canterbury Plains (Salinger, 1980) because the mountain ranges over the country play a significant control on precipitation patterns even for low relief areas (Watts, 1947).

Orographic enhancement of AR-induced precipitation in New Zealand has been recently investigated by several studies (Little et al., 2019; Porhemmat et al., 2020; Prince et al., 2021; Reid et al., 2021; Shu et al., 2021) as well as the connection between historical flood events and ARs (Kingston et al., 2016). Generally, ARs are the main contributor to annual rainfall and responsible for many extreme rainfall events on the western areas of mountain ranges throughout the country (Shu et al., 2021). However, as noted in Reid et al. (2021), at least 8/10 of the top historical rainfall events show association with AR activities for some rain sites located in the eastern areas of mountain ranges, despite the percentage of AR-induced extreme rainfall events being relatively low in such areas (Shu et al., 2021). It should also be noted that most ARs commonly make landfall along the west coast with a northwest orientation, while ARs can approach the east coast with a northeast orientation in some cases (Prince et al., 2021; Shu et al., 2021). Therefore, the spatial distribution of AR-induced rainfall is likely to be related to an AR's orientation, considering that the role of cyclones and fronts in generating heavy rainfall events (Catto & Pfahl, 2013; Pfahl & Wernli, 2012) and the windward side of mountain ranges being favourable for anomalously high precipitation over the country (Salinger, 1980).

The different landfall directions of ARs can lead to variable daily rainfall amounts (Hecht & Cordeira, 2017). Following the work by Shu et al. (2021), in this study, the characteristics of ARs in association with the two main orientations (northwesterly and northeasterly) and four different AR landfall directions and the corresponded pattern of AR-induced rainfall will be examined in detail over New Zealand. In addition, the applicability of a slightly modified AR impact ranking scale initially developed by Ralph et al. (2019) for the U.S. west coast will be evaluated considering the diverse orography and regional-specific weather processes in New Zealand. The present study is organised as follows. Section 2 describes the collected data, AR detection algo-

rithm, AR impact ranking scale, AR-rain identification method, and divided sectors in terms of "AR impact", according to Shu et al. (2021). Section 3 presents results regarding the characteristics of landfalling ARs in terms of their different orientations and landfall directions. Section 4 and 5 demonstrate that the spatial distribution of AR-induced heavy rainfall controlled by AR-event orientation and mean landfall direction varies with "AR impact" sector. Section 6 evaluates the applicability of the modified AR impact ranking scale with respect to different AR orientations and mean landfall directions for different "AR impact" sectors. Finally, Section 7 provides a summary.

2 Data and Methods

2.1 Data

AR detection is based on the integrated water vapour transport (IVT) magnitude from an Eulerian framework (Blamey et al., 2018; Lavers et al., 2012; Nayak & Villarini, 2017), which is given by:

$$\mathrm{IVT} = \sqrt{\left(\frac{1}{g}\int_{1000\mathrm{hPa}}^{300\mathrm{hPa}} \mathrm{qu}\ \mathrm{dp}\right)^2 + \left(\frac{1}{g}\int_{1000\mathrm{hPa}}^{300\mathrm{hPa}} \mathrm{qv}\ \mathrm{dp}\right)^2}, \quad (1)$$

where q is specific humidity (kg kg^{-1}), u and v are zonal and meridional wind vectors (m s^{-1}) respectively, g is the gravitational acceleration (9.81 m s^{-2}), and dp is the pressure difference between two adjacent atmospheric pressure levels (hPa). To compute IVT, 20 vertical pressure levels (1000hPa-300hPa) of 6-hourly specific humidity and wind vectors were retrieved from the European Centre for Medium-Range Weather Forecasts (ECMWF) Interim (ERA-interim) (Dee et al., 2011) from 1979 to 2018 with a 0.125° spatial resolution over the 0-70°S and 100°E-120°W domain. To compare the Interim-based landfalling AR characteristics, ARs detected globally from the Climate Forecast System Reanalysis (CFSR) (Saha et al., 2010) were retrieved from a global AR database with 0.5° horizontal grid spacing from 1979 to 2015 (Guan & Waliser, 2015). Note that only ARs which make landfall along New Zealand coastlines were considered in this study.

Station-based daily rainfall amounts were obtained from New Zealand's national climate database web system managed by the National Institute of Water and Atmospheric Research (NIWA). To avoid an inaccurate estimate of the spatiotemporal connection between ARs and rainfall and consider the coverage of sites over the country, 655 stations with 100% completeness and at least a 10-year length between September 1979 to August 2018 were selected. Note that the data length differs among sites, and the maximum and mean length of all sites is 39 and 19 years, respectively.

2.2 AR detection

The AR detection algorithm developed by Guan and Waliser (2015) was employed in this study, which involves a set of conditions on the IVT grid cells to identify AR objects every time step within the specified domain. The AR object

refers to the instantaneous area that meets the defined AR detection conditions. The detection conditions include grided IVT magnitude thresholding, the poleward direction of the AR object, IVT direction coherence within the AR object, consistency between the AR-object mean IVT direction and orientation, and the AR-object geometry. Detailed AR detection procedures and conditions are provided in Guan and Waliser (2015). Archived landfalling AR dates from this algorithm shows over 90% agreement with other regional-specific AR detection techniques (Gorodetskaya et al., 2014; Guan et al., 2018; Lavers et al., 2012; Neiman et al., 2008; Ralph et al., 2019; Shields et al., 2018) and this algorithm was only the one that has been validated from the dropsonde observations for the AR intensity and geometry. Thus, this algorithm has been widely used as a benchmark in different regions for AR tracking studies (Guan & Waliser, 2019; Zhou et al., 2018; Zhou & Kim, 2019) and regional-specific AR detection algorithm development (Gershunov et al., 2017; Pan & Lu, 2019; Reid et al., 2020). Note that landfalling AR dates and landfall locations were obtained and archived from the algorithm as well as the corresponding AR characteristics in New Zealand, and the landfalling AR characteristics selected in this study are: AR length and length/width ratio, AR direction coherence, AR IVT magnitude and direction at landfall, and AR orientation. Note that landfalling AR orientations are northwesterly and northeasterly in New Zealand (Shu et al., 2021), but the landfall direction can be any direction. To evaluate the association of rainfall patterns with differently orientated and directed ARs, detected landfalling ARs were grouped in terms of their orientations and landfall directions (Figure 1). For example, as shown in Figure 1a, a northwesterly orientated landfalling AR with a southwesterly landfall direction is denoted as an NW-SW AR.

2.3 AR impact ranking scale

An AR impact ranking scale was initially developed by Ralph et al. (2019) to categorise an AR's impact by the AR-event peak IVT magnitude and duration over the location of interest. Briefly, the IVT and duration intervals for categorising an AR event rank is 250 kg m^{-1} s^{-1} and 24 hours, respectively. A detailed description of the ranking scale is in Ralph et al. (2019). It should be noted that the AR impact ranking scale used in this study is slightly different (Table 1) since the AR detection algorithm by Guan and Waliser (2015) enables ARs with IVT less than 250 kg m^{-1} s^{-1}, removing the threshold to first identify an AR event (i.e., Ralph et al., 2019). In this study, AR events with a peak IVT magnitude less than 250 kg m^{-1} s^{-1} were ranked in the low IVT AR category (also see Prince et al., 2021).

Table 1. A modified AR impact ranking scale applied in this study for New Zealand ARs.

AR-event peak IVT (kg m^{-1} s^{-1})	Duration of AR event (hours)		
	24	>24-48	>48

AR-event peak IVT (kg m^{-1} s^{-1})	Duration of AR event (hours)		
250	Low IVT AR	Low IVT AR	Low IVT AR
>250-500	Weak AR	Cat1 AR	Cat2 AR
>500-750	Cat1 AR	Cat2 AR	Cat3 AR
>750-1000	Cat2 AR	Cat3 AR	Cat4 AR
>1000-1250	Cat3 AR	Cat4 AR	Cat5 AR
>1250	Cat4 AR	Cat5 AR	Cat5 AR

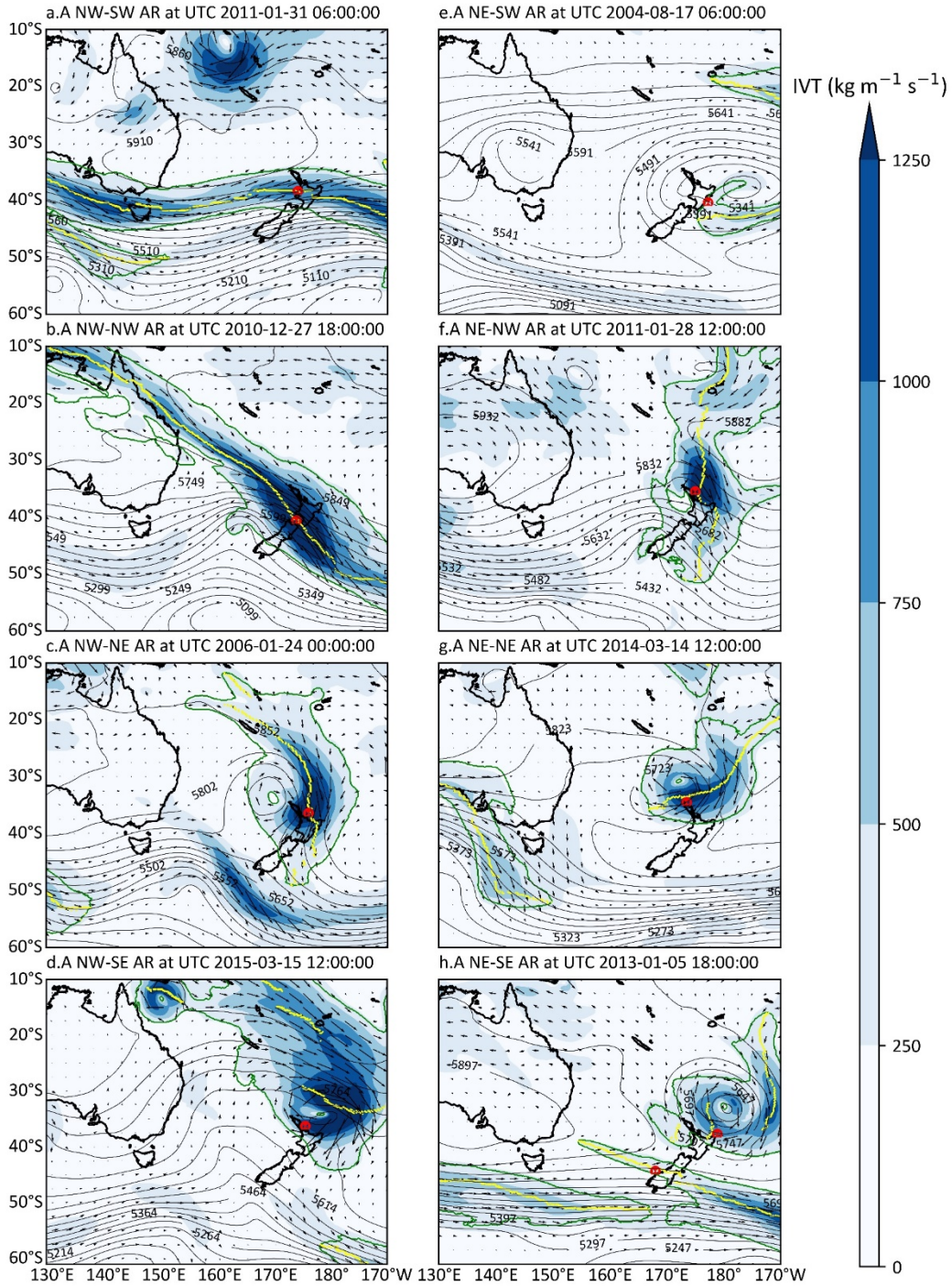

Figure 1. Detected ERA-Interim ARs with different orientations and land-

fall directions. The outcomes of the AR detection algorithm include the shape boundary (green), axis (yellow), landfall location (red dot). The area shaded in blue and arrow vectors refer to the AR magnitude (kg m^{-1} s^{-1}) and direction at each grid point, superimposed with 500-hPa geopotential height (contours on a 50-m interval). **a-d** Northwesterly orientated ARs with 4 different landfall directions: southwest (NW-SW), northwest (NW-NW), northeast (NW-NE) and southeast (NW-SE). **e-h** Same as **a-d** but for northeasterly orientated ARs.

2.4 AR-induced rainfall events

We modified the method used to identify AR-induced rainfall events in Shu et al. (2021). Based on the geographical coordinate of the 4 grid points enclosing a rain gauge, the date and time that all 4 points simultaneously detected AR activities were referred to an AR event at that date and time for that rain gauge. The start and end date and time of each AR event were then calculated, and duration was computed accordingly. The areal mean IVT and mean direction of each AR event at each time step were computed, and the peak IVT and mean direction over all time step(s) within the AR-event duration were further computed. To link AR events with archived landfalling ARs, the beginning of each AR event was checked with the landfalling AR date-time archive and only AR events that the mean direction matched the AR's landfall direction were considered for analysis in Sections 4-6. This is because it is possible to detect more than one landfalling AR over the country (Figure 1h) for any timestep. Moreover, the peak daily rainfall amounts and the standardised index of each AR event were obtained, and the index was calculated as:

$$\text{Standardised index} = \frac{x-\overline{x}}{S}, \quad (2)$$

where x is the AR-event peak daily rain amount, $\overline{x}$ is the annual mean daily rainfall, S is the annual daily rain standardised deviation. Following the work done by Shu et al. (2021), areas that experience higher AR's contribution to annual rainfall tend to see a higher proportion of top 10% heavy rainfall events linked with ARs (Figures 2a-c). To further evaluate the pattern of AR-induced extreme rainfall events in New Zealand, the country was divided into 4 sectors in terms of "AR impact": the East Coast and the West Coast, based on certain thresholds of AR's contribution to annual rainfall and top 10% of rainfall events (Figure 2d).

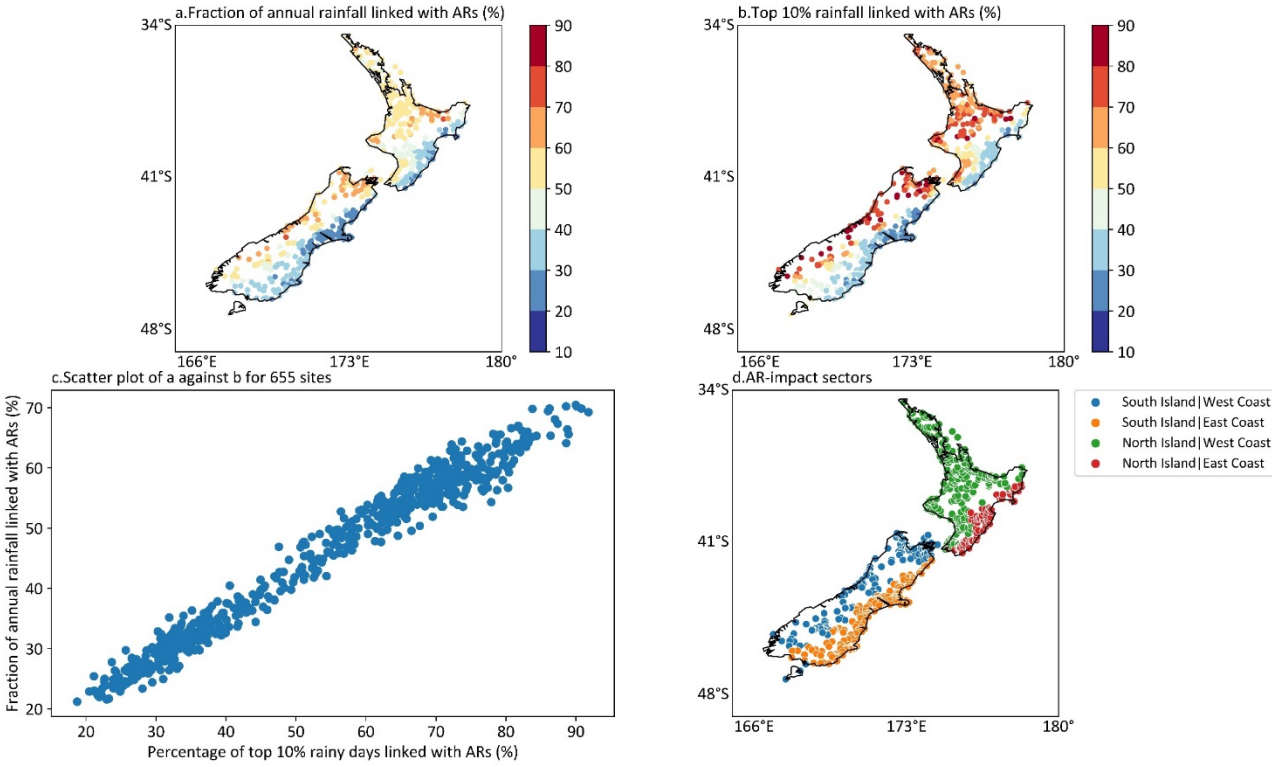

Figure 2. Contribution of ARs to annual rainfall and extreme rainfall events, and the divided sectors in terms of "AR impact". **a** Mean fraction of AR-induced annual rainfall. **b** Mean proportion of extreme daily rainfall events (greater than 90th percentile value) linked with ARs. **c** Mean AR's contribution to annual rainfall against the mean percentage of AR-induced extreme rainfall events for each rain gauge. **d** Divided "AR impact" sectors according to c, divide includes the South Island and North Island combined with the West Coast and East Coast; East Coast refers to where AR's contribution to annual rainfall less than 41% and to top 10% rainfall less than 50%, and its counterpart is the West Coast.

3 Characteristics of landfalling ARs with different orientations and landfall directions

Characteristics of ERA-interim landfalling ARs with 2 main orientations and 4 landfall directions are shown in Figure 3 and Table 2. Equivalent results for CFSR are provided in Supplementary Figure S1 and Table S1. The occurrence of NW-NW ARs is notably high, whereas NE oriented ARs rarely occur (Tables 2 and S1). The notable difference in the occurrence of NW-NW ARs and other ARs reflect the dominant weather process in New Zealand: mid-latitude cyclones embedded within the westerlies (Salinger, 1980; Sinclair, 1994; Tait & Fitzharris,

1998; Watts, 1947). Generally, for ARs that with the same landfall direction and orientation tend to have relatively higher landfall IVT magnitude, direction coherence, and length/width ratio (Figures 3c-f; Figures S1c-f), reflecting the concentrated corridors of enhanced water vapour flux within these ARs than other ARs which are somewhat disturbed or modified (Figure 1). The length is relatively higher for ARs with an SW landfall direction (Figures 3d-e and S1d-e) since NW-SW ARs might travel from the northwestern regions near Australia (Figure 1a) and detected NE-SW ARs might split from NW ARs over the ocean basin (Figure 1b).

Table 2. Occurrence (probability %) of detected landfalling ARs from ERA-Interim

AR orientation	IVT direction at landfall location			
	SW	NW	NE	SE
NW	1511 (8.5%)	14070 (78.7%)	1303 (7.3%)	117 (0.7%)
NE	6 (0.03%)	111 (0.6%)	662 (3.7%)	96 (0.5%)

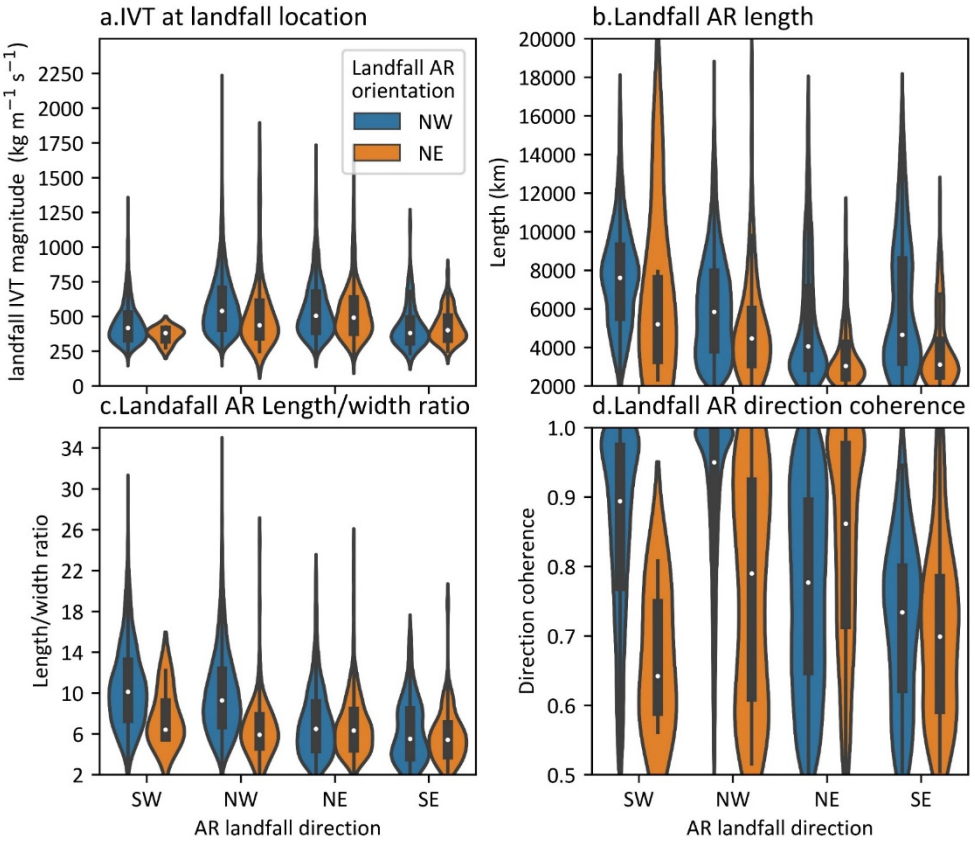

Figure 3. Characteristics of ERA-Interim based landfalling ARs with different orientations and landfall directions. **a-b** The occurrence and proportion of ARs. **c-d** IVT magnitude, length, length/width ratio, and direction coherence, at landfall location, respectively.

The AR landfall location is likely to be controlled by the largest pressure gradients (Prince et al., 2021). For example, low pressure in the Tasman Sea to the northwest of the country, with a high pressure positioned farther south, can potentially draw the moisture from the subtropics via the resultant winds (Figures 1c and 1g). Thus ARs make landfall on the northern coast of the North Island. The spatial distribution of ERA-interim landfalling AR occurrence and corresponding landfall locations is illustrated in Figure 4 (CFSR equivalent provided in Supplementary Figure S2). The pattern of landfall location and windward side are controlled by the orientation and landfall direction of ARs. For example, NW-NW ARs make landfall along the west coast of the country and the north coast of the North Island, while NE-NE ARs make landfall along most coastlines of the country (Figures 4b and g, Figures S2b and g). Overall, NW ARs show notably high occurrence along the west coast over the country and the north coast of the North Island. In contrast, NE ARs show relatively high occurrence on the east coast. Additionally, a higher maximum IVT magnitude at landfall location is more likely to be associated with NW ARs than NE ARs (Figures 4i-p and S2i-p).

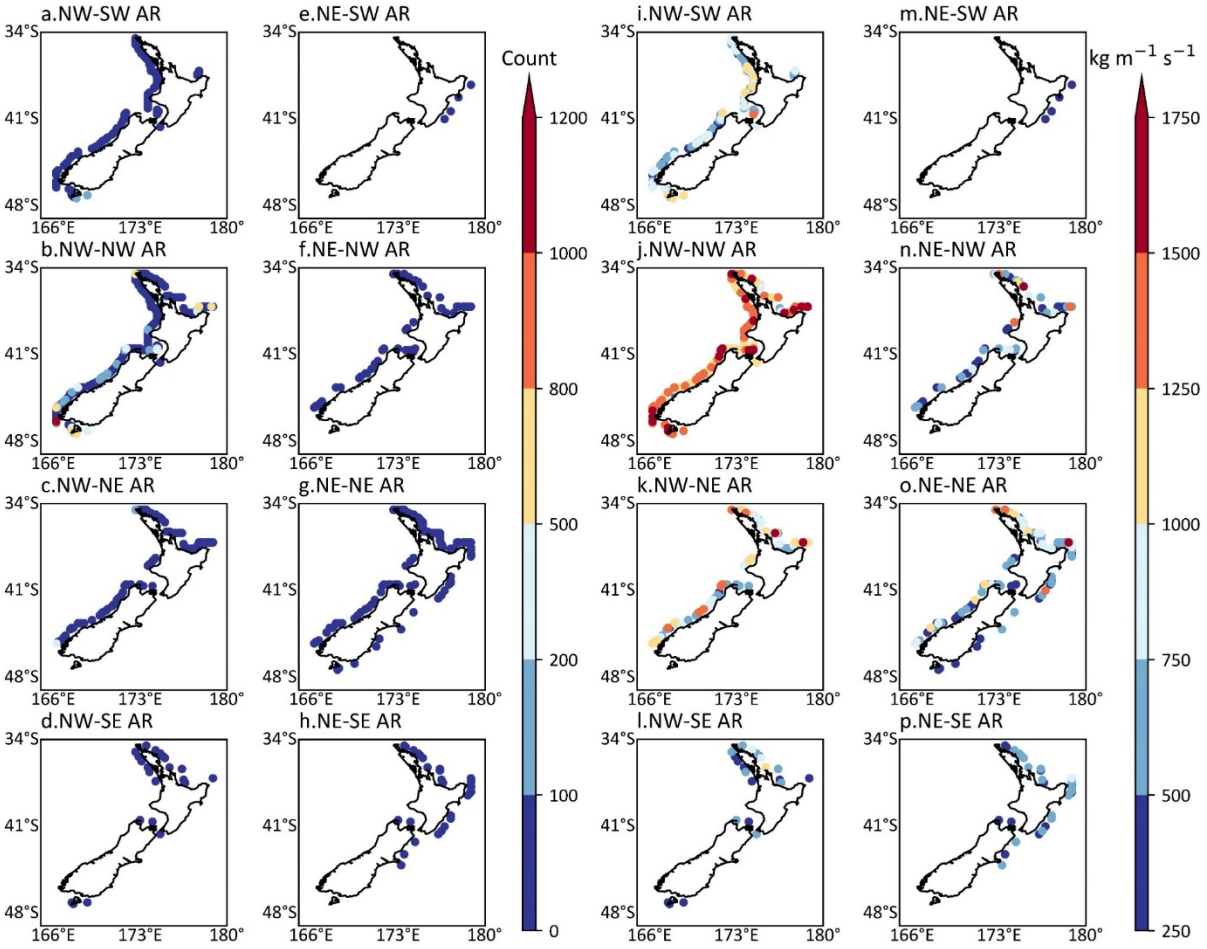

Figure 4. Spatial distribution of landfall locations for ERA-Interim based ARs along the coastline and corresponding occurrence (**a-h**) as well as maximum IVT magnitude (**i-p**).

4 AR-induced rainfall patterns

4.1 Spatial distribution of AR's contribution to annual rainfall

A northwesterly landfalling AR with a southwesterly landfall location leads to an AR event with a mean southwesterly direction among rain gauges denotes an NW-SW AR event for affected sites (e.g. Figure 5a). Figure 5 shows the spatial distribution of AR-event contribution to annual rainfall and the frequency of each category of AR event. NW-NW AR events, as expected, show the greatest frequency over the country, resulting in the most significant contribution to annual rainfall. Due to the orographic lifting effect, NW-NW ARs make a higher rain-total contribution on the western side of the mountain ranges. The results here agree with recent work (Prince et al., 2021; Reid et al., 2021; Shu

et al., 2021) and further highlight the dominant role of NW-NW ARs on water resources over the western areas of mountain ranges in the country and the northern North Island.

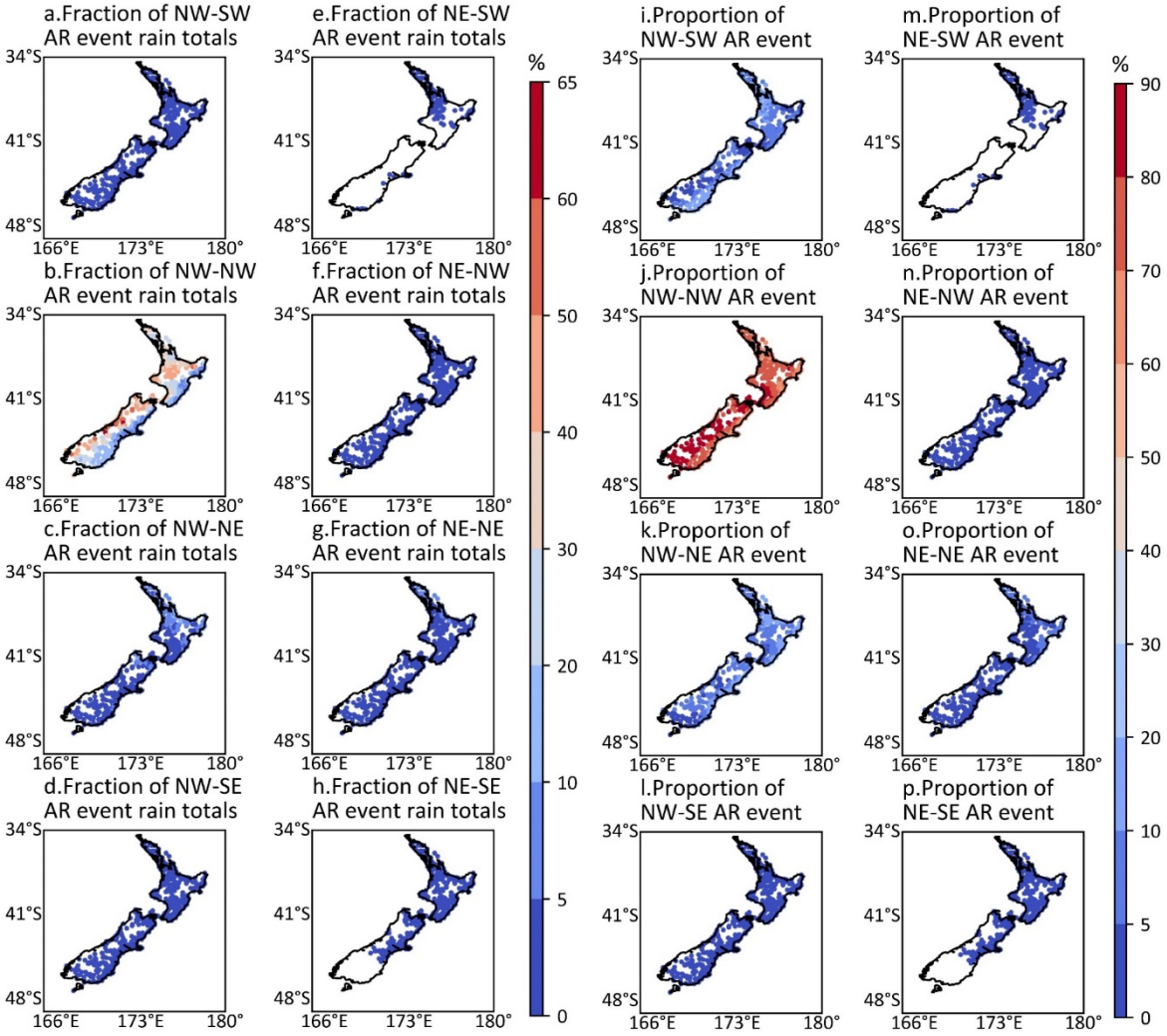

Figure 5. Fraction of AR-event rain totals over annual rain totals and percentage of AR-event occurrence with different orientations and mean landfall directions over total AR-event occurrence. **a-h** AR's contribution to rainfall totals. **i-p** AR's occurrence in percentage.

4.2 Spatial distribution of AR-event extreme rainfall

The pattern of the 90th percentile of AR-event peak daily rain amount is broadly controlled by an AR's orientation and landfall direction as well as the orientation of mountain ranges over the country (Figure 6). NW-SW ARs do not generally

lead to heavy rainfall (Figure 6a) but can cause anomalously high rainfall (for that location) on the eastern side of mountain ranges (Figure 6e). Shown in Figure 1a and Figure 1h is an example of NW-SW reaching the country when the westerlies cover the country and move the south of the country, respectively. Rainfall sourced from NE-SW ARs only occurs on the upper central part of the North Island and can lead to heavy rainfall for some areas (Figures 6i and 6m). These ARs might originate and split from an NW AR through its lifetime before reaching New Zealand, seemingly through interaction with cyclonic activity (Figure 1e). Heavy rainfall caused by NW-NW AR events tends to concentrate on the western side of the Southern Alps and Mount Taranaki because of the substantial enhancement of orographic precipitation. In comparison, NE-NW ARs are more northerly orientated and tend to cause heavy rainfall for most North Island sites (except in the south) and the west and upper-north of the Southern Alps (Figures 6b and j). Note that the standardised index is relatively high on the windward side (Figures 6f and n), especially the upper-central North Island (Figure 6n), although NE ARs are generally weaker than NW ARs (Figures 3-4 and S1-2).

When westerlies move further south, ARs are more likely to approach the country with a NE or SE landfall direction and associate with cyclones (Figures 1c-d and g-h). Via rotation when interacting with cyclonic activity and directed northerly towards the country (Figures 1c and g), both NW-NE and NE-NE ARs can lead to heavy rainfall along most coastlines apart from southern parts of both islands, as well as anomalously high rainfall for the northern and central-eastern North Island and eastern South island (Figures 6c,g,k,o). Additionally, some southern South Island locations observed high rainfall when landfalling NE-NE ARs occurred (Figure 6o). When ARs tend to be orientated easterly and make landfall with a SE direction, eastern regions are now on the windward side and receive anomalously high rainfall (e.g. Figures 6h and p). The orientation of AR events broadly determines the pattern of heavy rainfall, and the enhanced orographic rainfall can occur on the east coast when ARs reach the county with SE direction (Figures 6h and p). Note that both locally highest 90th percentile rainfall and standardised index occur when ARs make landfall with a SE direction over eastern regions. This is particularly true given that the mean airflow over the country is from the west, and ARs generally rain out on the western portions of the mountain ranges. However, one synoptic-scale event that causes moisture air flows westward from the east or northeast can cause the highest rainfall locally (Salinger, 1980).

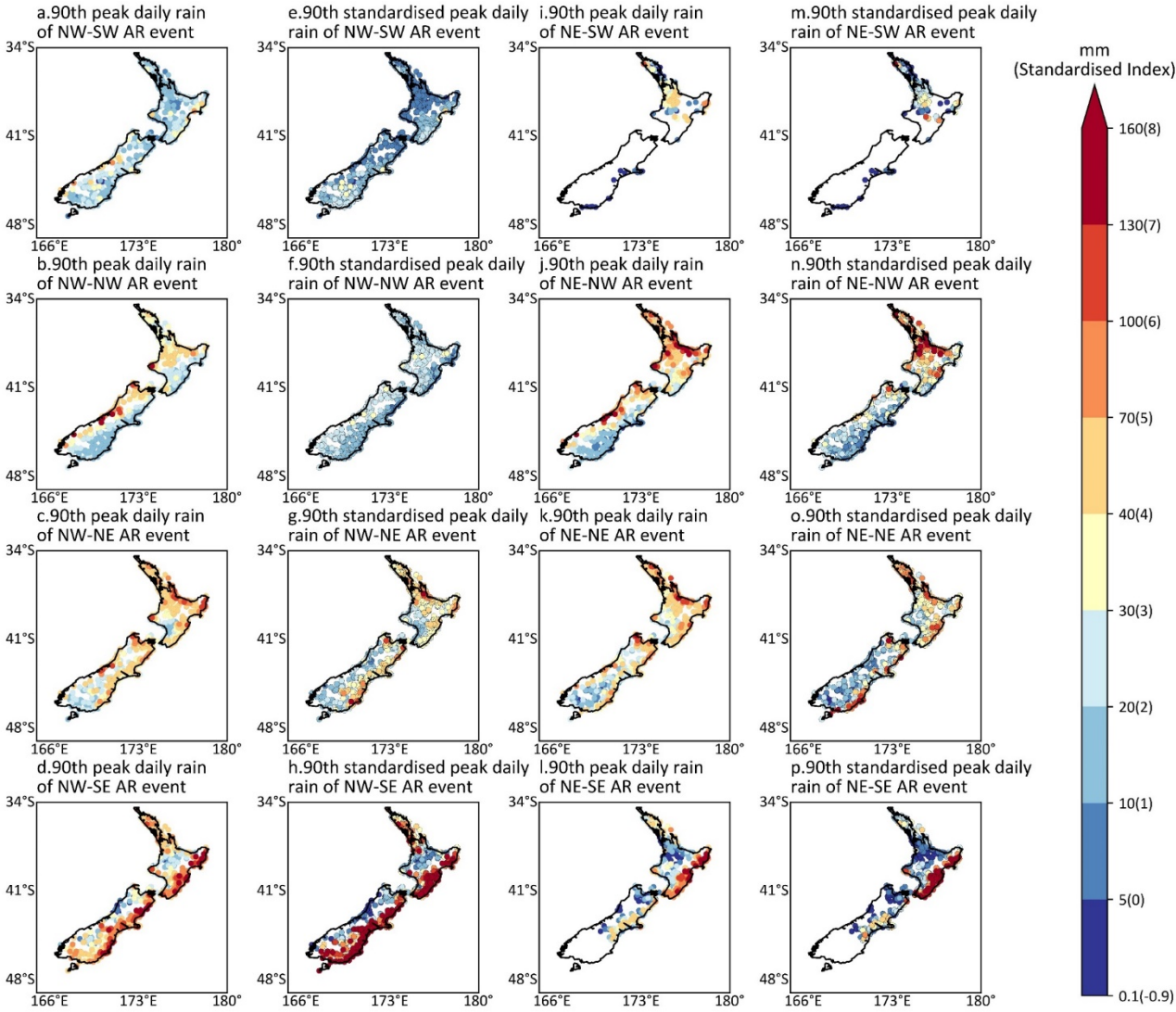

Figure 6. 90th percentile value of northwesterly oriented AR-event (**a-d**) peak daily rainfall amount and (**e-h**) corresponding standardised index with different mean landfall directions. (**i-l** and **m-p**) Same as **a-d** and **e-h** but for northeasterly orientated ARs.

5 Distinct AR-event rainfall in different AR-impact sectors

Figures 7 and 8 illustrate the statistical distribution of AR-event peak daily rainfall that correspond to a standardised index greater than 1. All rainfall sourced from AR events is grouped by the "AR impact" sector described in Section 2, the AR orientation, and the mean AR-event IVT direction for each AR event. The East Coast of both islands is more likely to see anomalously high

rainfall amount than the West Coast when AR events have a mean SE direction. In contrast, the largest AR-induced daily rainfall is likely to occur on the West Coast for both islands when NW-NW ARs occur, with the highest anomalous rainfall amounts observed to be about 660 mm (South Island) and 500 mm (North Island). Nevertheless, NW-NW ARs can also produce anomalously high rainfall on the East Coast, although rainfall is generally lower than on the West Coast. The spatial rainfall pattern associated with AR events with a mean NE direction is similar for both NW and NE ARs over the country since the wind shifts from northwest to northeast. During such events, the windward side is now the eastern side, resulting in higher rainfall on the East Coast when AR events have a mean SE landfall direction. Rainfall associated with NE-AR events generally display a similar pattern with NW-AR events, but the rainfall amount is generally lower than NW-AR events within the same landfall direction zone. This is presumably due to NW ARs generally being stronger than NE ARs (Figures 3 and S1). However, NE-AR events can also lead to anomalously high rainfall over the country. Overall, the anomalously high rainfall usually occurs on the windward side over the country, and thus the AR orientation and the AR-event mean landfall direction together play a role in determining where such heavy rainfall will be experienced in New Zealand.

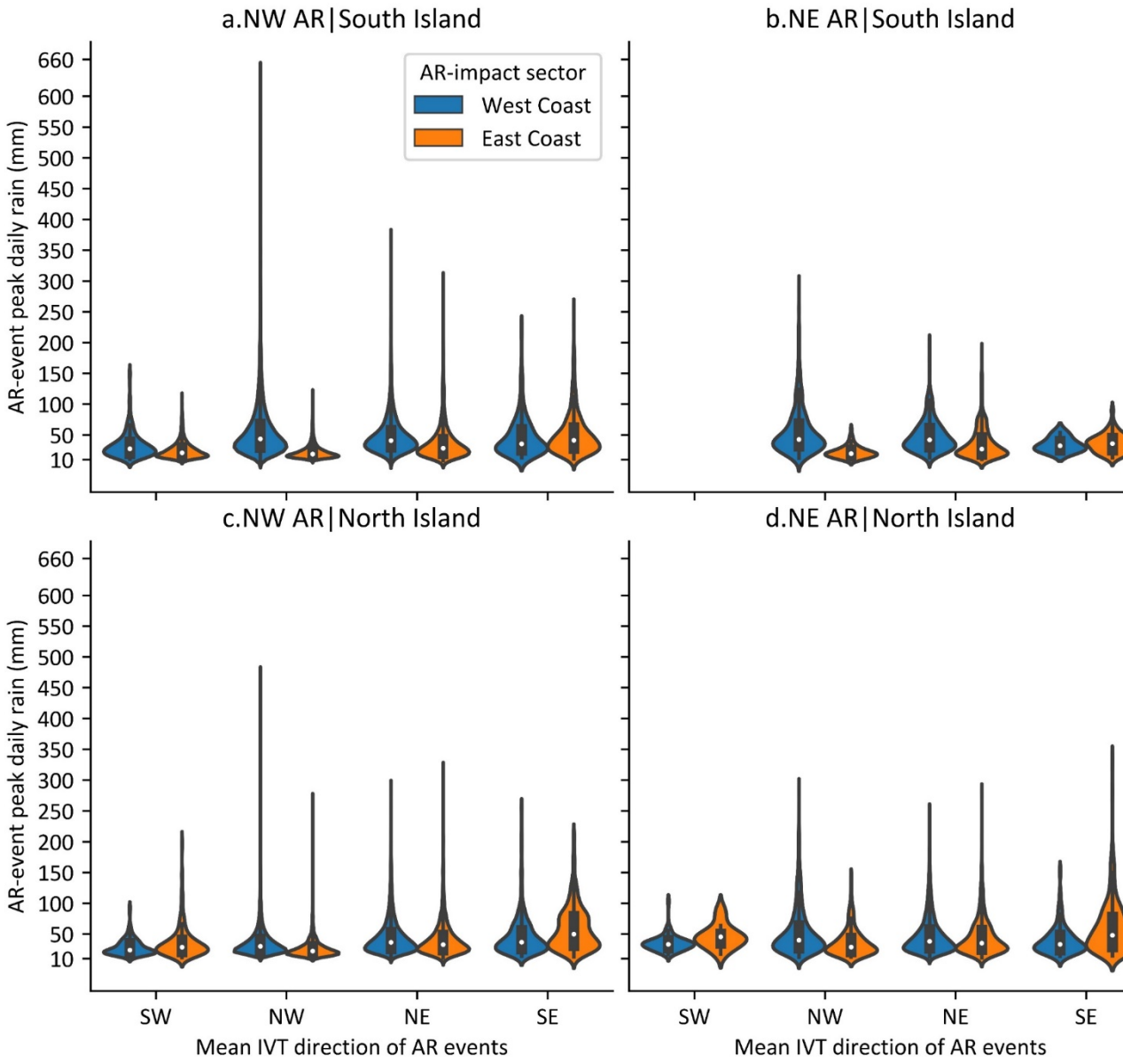

Figure 7. All AR-event peak daily rainfall amount in terms of different AR-event orientations and mean landfall directions as well as "AR impact" sectors in both islands of New Zealand. Note that only rainfall with a standardised index greater than 1 is considered.

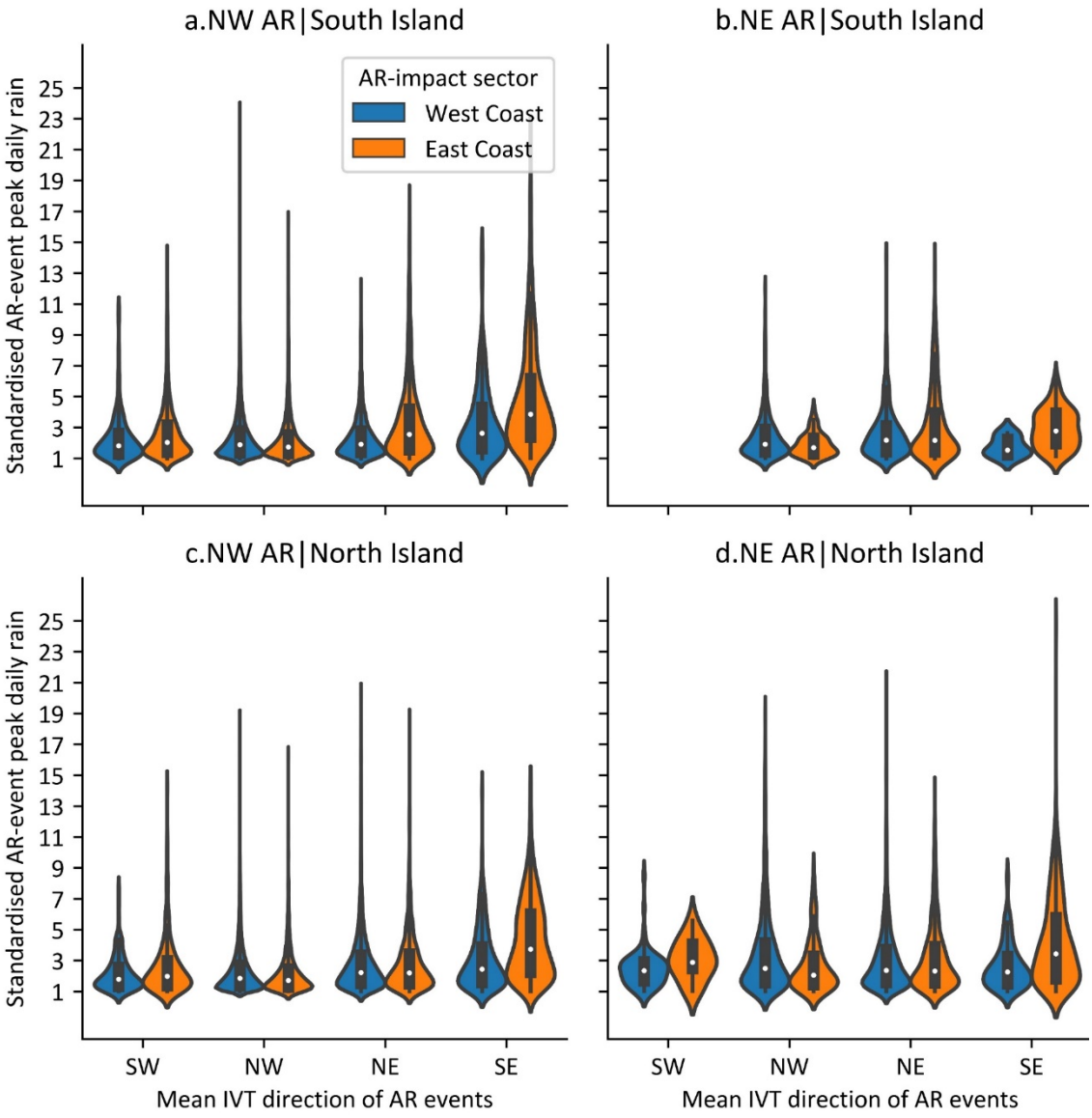

Figure 8. Same as Figure 7 but for standardised AR-event peak daily rainfall.

6 The applicability of AR ranking scale in New Zealand

The peak IVT magnitude of an AR event is one of the parameters commonly used to rank the impact of an AR (Ralph et al., 2019; Prince et al., 2021), as shown in Table 2. Figures 9 and 10 illustrate the AR-event peak daily rainfall amount and its standardised index regarding AR orientation, mean AR-event direction, "AR impact" sectors, and AR-event peak IVT magnitude. Similar to Figures 7 and 8, the anomalously high rainfall pattern is broadly controlled by

the AR orientation, landfall direction, and orographic uplift compared to the peak IVT magnitude of AR events. The East Coast of the country generally receives anomalously higher rainfall than the West Coast when AR events have an easterly landfall direction, although higher IVT magnitude is evident on the West Coast (Figures 9c-d). Extreme rainfall sourced from NW-NW ARs appears to concentrate on the West Coast of the South Island, while NW-NW and NW-NE ARs can lead to extreme rainfall on the West Coast of the North Island, as it includes northern North Island and northern coast. Likewise, some anomalously high rainfall appears to coincide with NE AR events over the country.

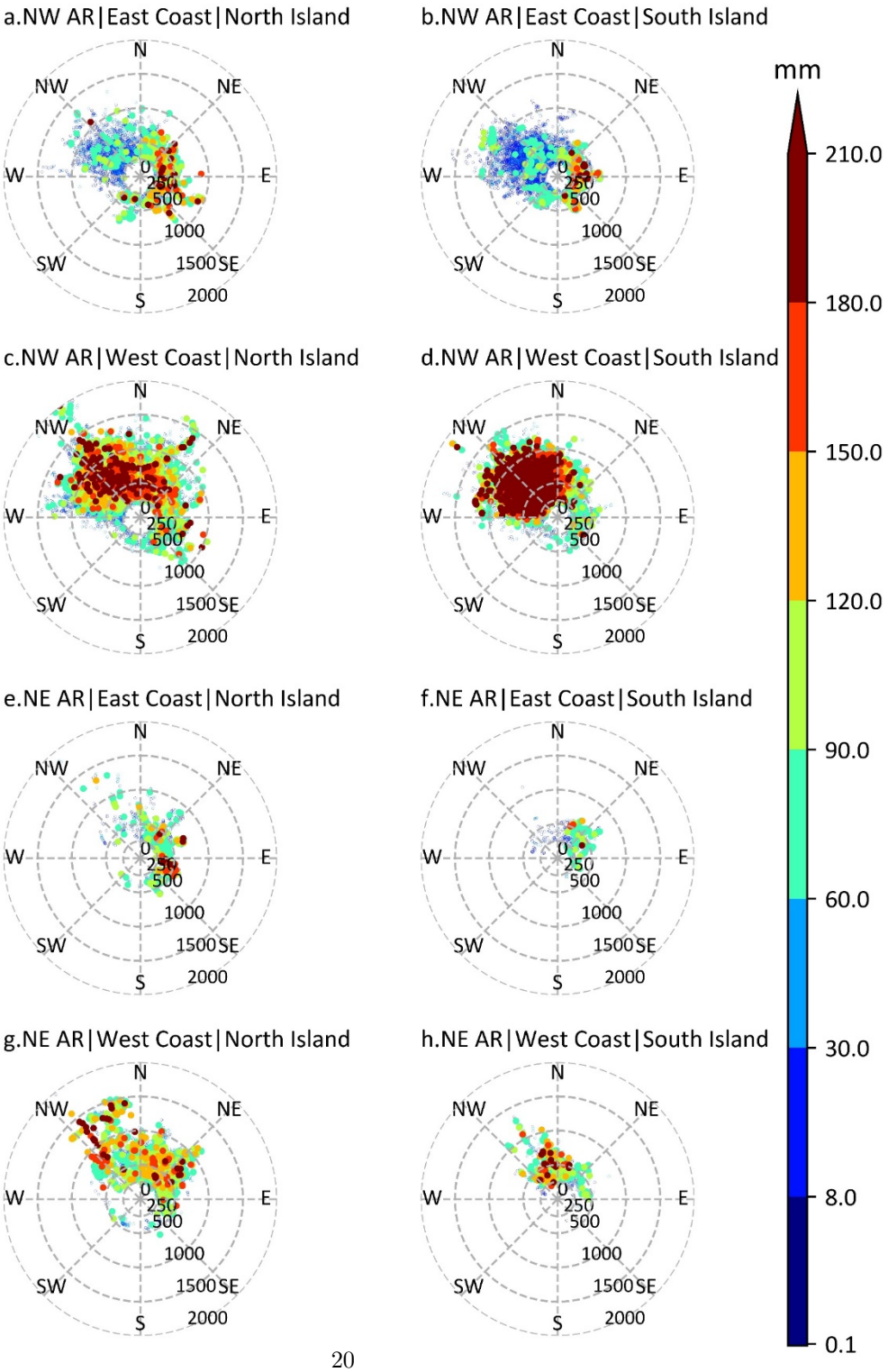
a.NW AR|East Coast|North Island
b.NW AR|East Coast|South Island
c.NW AR|West Coast|North Island
d.NW AR|West Coast|South Island
e.NE AR|East Coast|North Island
f.NE AR|East Coast|South Island
g.NE AR|West Coast|North Island
h.NE AR|West Coast|South Island
N
NE
E
SE
S
SW
W
NW
0
250
500
1000
1500
2000
mm
210.0
180.0
150.0
120.0
90.0
60.0
30.0
8.0
0.1

Figure 9. AR-event peak daily rainfall amount in relation to peak IVT magnitude (radial coordinate) for different AR-event orientations and mean landfall directions (angular coordinate) as well as "AR impact" sectors. Note that only rainfall with a standardised index greater than 1 is considered.

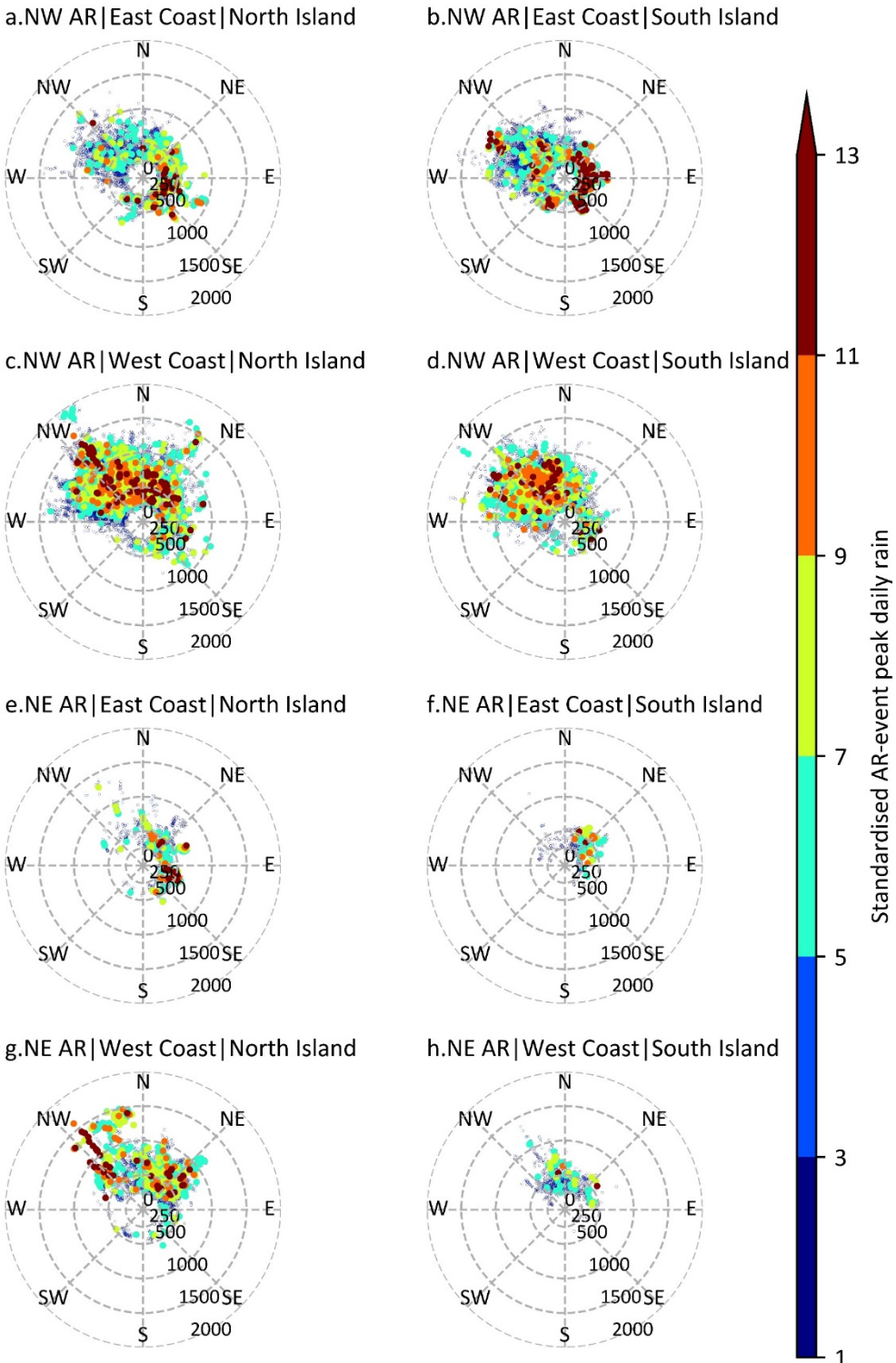
a.NW AR|East Coast|North Island
b.NW AR|East Coast|South Island
c.NW AR|West Coast|North Island
d.NW AR|West Coast|South Island
e.NE AR|East Coast|North Island
f.NE AR|East Coast|South Island
g.NE AR|West Coast|North Island
h.NE AR|West Coast|South Island
N
NE
E
SE
S
SW
W
NW
0
250
500
1000
1500
2000
Standardised AR-event peak daily rain
1
3
5
7
9
11
13

Figure 10. Same as Figure 8 but for the standardised index of rainfall.

Considering that AR's orientation and landfall direction play a role in determining where locally heavy rainfall is likely to occur, we further evaluate the applicability of the AR-impact ranking scale in Table 1 concerning AR-event orientation and mean direction (Figures 11-12 and S3-S4). Note that only rainfall with a standardised index greater than 1 is considered. The ranking scale generally performs better for NW ARs than NE ARs. For example, the AR-event peak daily rainfall of NW-NW ARs follow the ranking scale for the West Coast over the country, and somewhat for the NW-NE ARs, whereas NW-SE ARs follow the scale well for the East Coast (Figures 11-12 and S3-S4). In comparison, the ranking scale does not perform well for NE ARs except NE-NW ARs for the West Coast of the North Island. However, it should be noted that AR events that do not follow the ranking scale can also lead to anomalously high rainfall, especially on the East Coast. Therefore, more parameters need to be considered to improve the applicability of the ranking scale for forecasting heavy rainfall events caused by NE ARs. Overall, the AR-ranking scale performs well for ARs that cause the most considerable rainfall in the country in terms of extreme rainfall.

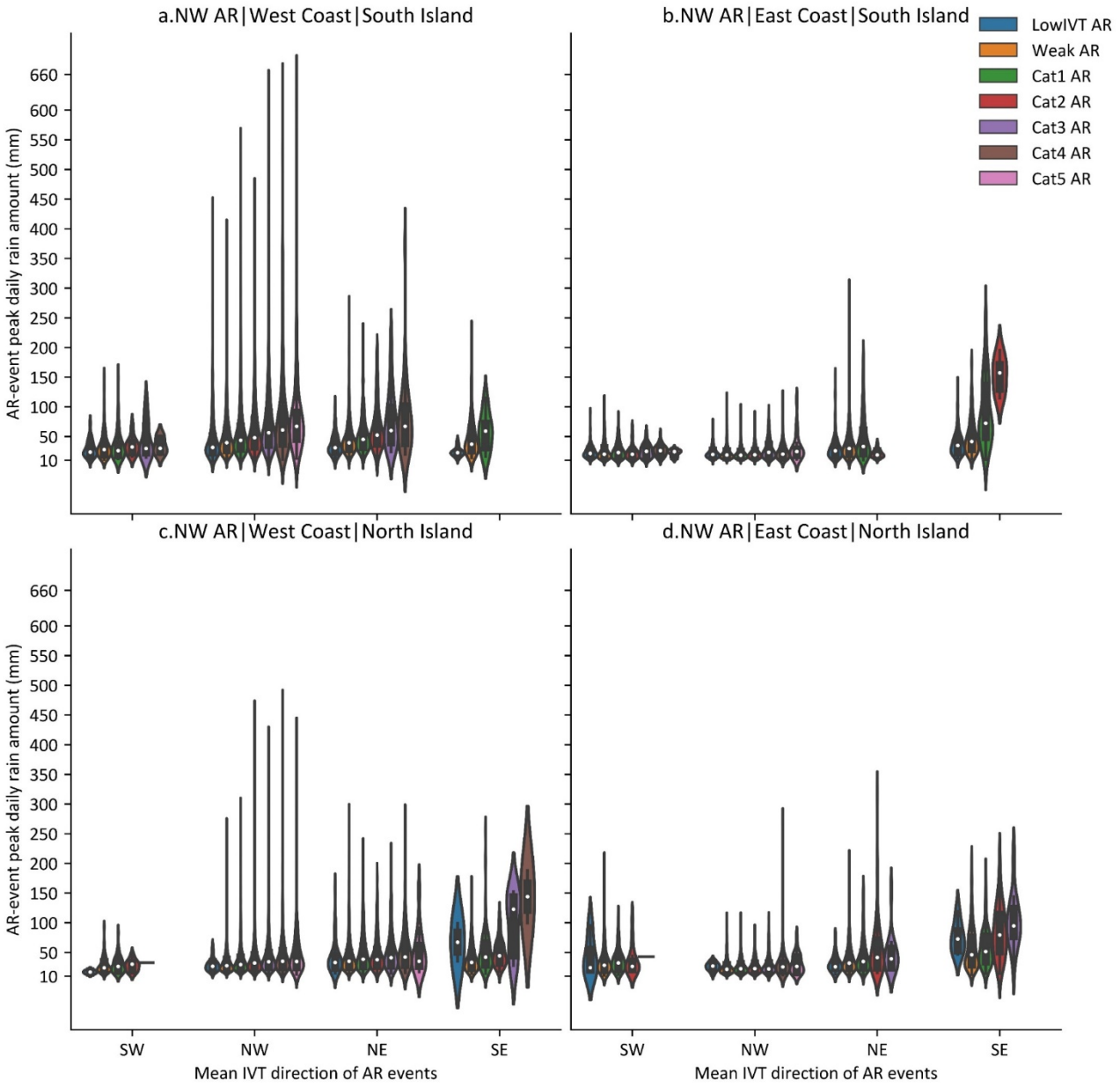

Figure 11. Distribution of AR-event peak daily rainfall amount for ranked NW AR events with different orientations and mean landfall directions at different "AR impact" sectors. Note that only rainfall with a standardised index greater than 1 is considered.

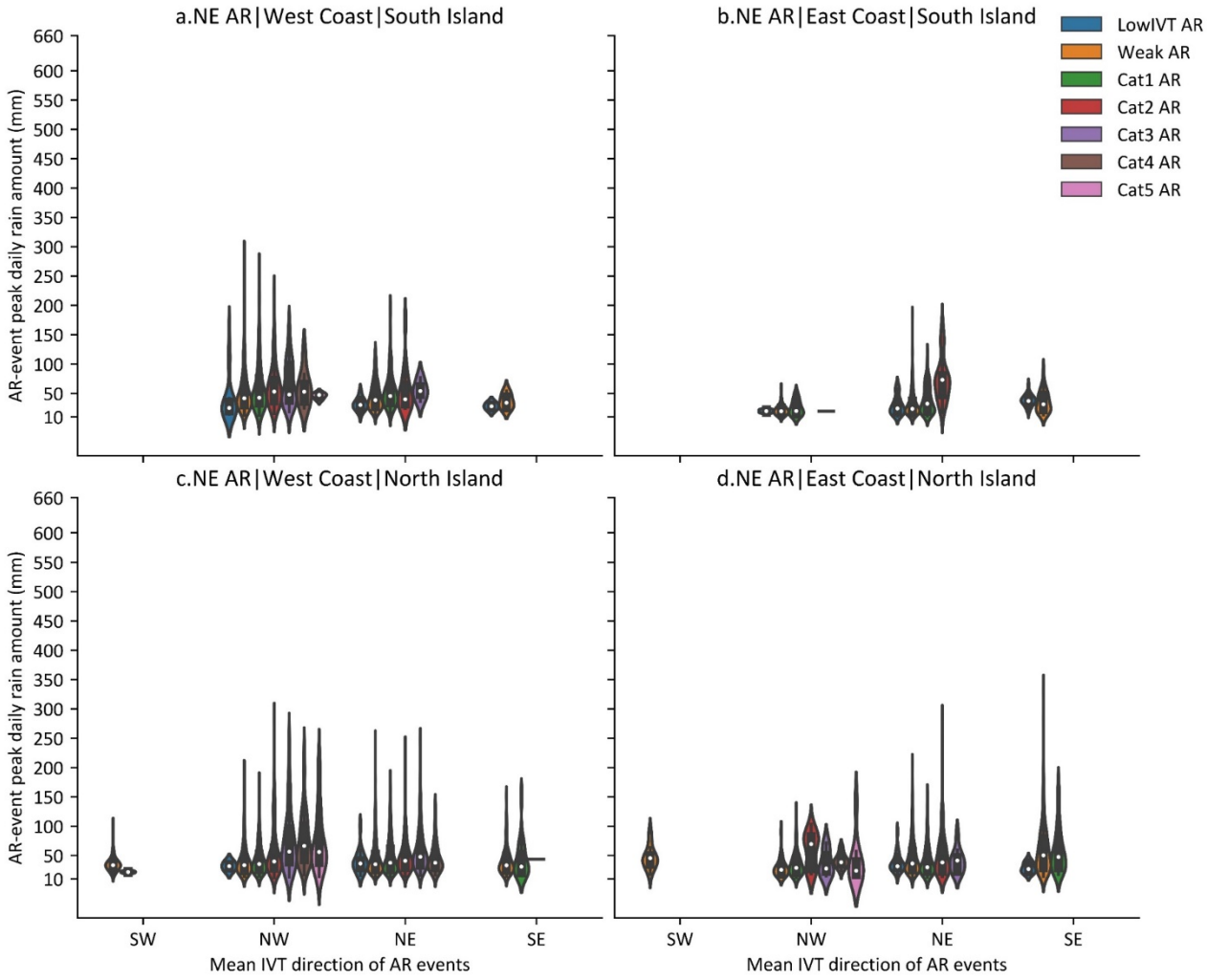

Figure 12. Same as Figure 11 but for NE AR events.

7 Conclusions

This study follows recent work to investigate further the pattern of heavy rainfall associated with AR events that have different orientations and landfall directions. Moreover, the applicability of a modified AR impact ranking scale originally developed by Ralph et al. (2019) was evaluated in New Zealand. Overall, landfalling ARs were detected based on the widely used AR detection algorithm by Guan and Waliser (2015) and the method used in Shu et al. (2021) to identify AR-event rainfall was modified to obtain characteristics of AR events among 655 rain gauges, including the start and end, duration, peak IVT magnitude, mean direction, orientation, event rank, and peak daily rain of each AR event among the rain gauge locations in New Zealand. Note that ARs were

detected based on 2 datasets (ERA-Interim and CFSR) to compare detected landfalling AR characteristics based on different reanalysis datasets. Following Shu et al. (2021), ERA-Interim ARs were employed for AR's impact analysis in Section 4-6, and the country was divided into 4 sectors in terms of "AR impact": the East Coast and the West Coast, according to Shu et al. (2021) (Figure 2). With this regard, the AR-induced rainfall pattern associated with AR-event orientation and mean landfall direction and the performance of the AR impact ranking scale were investigated.

We found that an AR's orientation and landfall direction, combined with mountain ranges' orientation, play a large role in determining the spatial distribution of heavy rainfall events over New Zealand. The major precipitation-generating weather systems are the westerlies and cyclones over the Tasman Sea and/or the tropical region due to the country's geographical location. The results indicate that most ARs are likely to associate with the westerlies over the country (Figure 1b) since NW-NW ARs occur the most, and some ARs are associated with cyclones embedded westerlies (Figure 1e) and tropical cyclones (Figure 1d). As a result, most ARs are NW-NW orientated-landfalling, of which are generally stronger, more coherent, and more concentrated than other ARs types. Due to the higher frequency of NW-NW ARs and the country's topography, the West Coast of the country (the windward side for NW-NW ARs) sees a relatively higher AR contribution to the annual total rain (Figure 5). The country's West Coast also receives the heaviest rainfall from NW-NW ARs, especially the West Coast of the South Island (Figure 7). Interestingly, heavy rainfall sourced from NE-NW AR events has a wider spatial distribution in the North Island than NW-NW AR events (Figure 6j). Over the 35 years examined, only NE-SW and NE-SE ARs appear to impact a certain part of the country (Figure 4). Hence, AR's orientation could be an important factor to determine where they produce heavy rainfall. With this regard, further study is needed to completely understand an AR's origin and lifecycle for forecasting the likely AR-induced rainfall.

An AR's landfall direction also plays a significant role in determining where the heaviest rainfall occurs. Generally, the windward side of the country experiences anomalously high rainfall. The West Coast and the East Coast of the country receive anomalously high rainfall when ARs make landfall with a mean AR-event NW and SE landfall direction, respectively. Likewise, most coastlines apart from the southern part of both islands experience anomalously high rainfall when AR events pass the country with a mean NE landfall direction. Considering the windward side is dependent on the AR's landfall location as well as the characteristics of ARs vary with its orientation and landfall location, the AR impact ranking scale was evaluated in terms of AR's orientation and landfall direction, divided sectors for both islands of the country, and the peak daily rainfall of each AR event. We found that the scale for NW-NW and NW-NE AR events (NW-SE AR events) perform well for the West Coast (East Coast) of the country. As for NE ARs, only NE-NW ARs follow the scale for the West Coast of North Island. Considering that the occurrence of extreme

rainfall on the West Coast is largely associated with NW-NW ARs, the ranking scale could be employed for AR-induced heavy rainfall forecasting. However, more characteristics (or atmospheric parameters) may be needed to forecast extreme rainfall for the East Coast because ARs with a NE landfall direction also produce heavy rainfall but do not follow the ranking scale well. As such, the association of ARs with dynamical weather processes such as cyclones is needed. Moreover, it should be noted that heavy rainfall can occur over a range of peak IVT magnitudes of each AR event. The relationship between the AR-event duration and associated peak daily rainfall was not investigated due to the temporal resolution being somewhat coarse for that needed (i.e., hourly to sub-daily), and thus one future focus could be for detailing AR-induced storms.

Acknowledgements

The authors thank NIWA for providing access to the New Zealand meteorological data from the National Climate Database, ECMWF for providing access to the ERA-interim dataset, and the Nectar Research Cloud for providing a cloud computing platform. The AR data and the AR detection code were provided by Bin Guan via https://ucla.box.com/ARcatalog. The development of the AR detection algorithm and databases was supported by NASA. This research is supported by the National Key Research and Development Program of China (grant no. 2016YFE0201900) and the State Key Laboratory of Hydroscience and Engineering (grant no. 2017KY04).

Data Availability Statement

Data used in this study were obtained freely online:

ERA-Interim:https://apps.ecmwf.int/datasets/data/interim-full-daily

Daily rainfall: https://cliflo.niwa.co.nz/

References

Blamey, R. C., Ramos, A. M., Trigo, R. M., Tomé, R., & Reason, C. J. C. (2018). The Influence of Atmospheric Rivers over the South Atlantic on Winter Rainfall in South Africa. *Journal of Hydrometeorology*, *19*(1), 127–142. https://doi.org/10.1175/JHM-D-17-0111.1Catto, J. L., & Pfahl, S. (2013). The importance of fronts for extreme precipitation. *Journal of Geophysical Research: Atmospheres*, *118*(19), 10,791-10,801. https://doi.org/10.1002/jgrd.50852Cordeira, J. M., Ralph, F. M., & Moore, B. J. (2013). The Development and Evolution of Two Atmospheric Rivers in Proximity to Western North Pacific Tropical Cyclones in October 2010. *Monthly Weather Review*, *141*(12), 4234–4255. https://doi.org/10.1175/MWR-D-13-00019.1de Kock, W. M., Blamey, R. C., & Reason, C. J. C. (2021). Large summer rainfall events and their importance in mitigating droughts over the south western cape, South Africa. *Journal of Hydrometeorology*, *22*(3), 587–599. https://doi.org/10.1175/JHM-D-20-0123.1Dee, D. P., Uppala, S. M., Simmons, A. J., Berrisford, P., Poli, P., Kobayashi, S., Andrae, U., Balmaseda, M. A., Balsamo, G., Bauer, P., Bechtold, P., Beljaars,

A. C. M., van de Berg, L., Bidlot, J., Bormann, N., Delsol, C., Dragani, R., Fuentes, M., Geer, A. J., … Vitart, F. (2011). The ERA-Interim reanalysis: configuration and performance of the data assimilation system. *Quarterly Journal of the Royal Meteorological Society*, *137*(656), 553–597. https://doi.org/10.1002/qj.828Dettinger, M. D. (2013). Atmospheric Rivers as Drought Busters on the U.S. West Coast. *Journal of Hydrometeorology*, *14*(6), 1721–1732. https://doi.org/10.1175/JHM-D-13-02.1Dettinger, M. D., Ralph, F. M., Das, T., Neiman, P. J., & Cayan, D. R. (2011). Atmospheric Rivers, Floods and the Water Resources of California. *Water*, *3*(2), 445–478. https://doi.org/10.3390/w3020445Gershunov, A., Shulgina, T., Ralph, F. M., Lavers, D. A., & Rutz, J. J. (2017). Assessing the climate-scale variability of atmospheric rivers affecting western North America. *Geophysical Research Letters*, *44*(15), 7900–7908. https://doi.org/10.1002/2017GL074175Gorodetskaya, I. V., Tsukernik, M., Claes, K., Ralph, F. M., Neff, W. D., & Van Lipzig, N. P. M. (2014). The role of atmospheric rivers in anomalous snow accumulation in East Antarctica. *Geophysical Research Letters*, *41*(17), 6199–6206. https://doi.org/10.1002/2014GL060881Guan, B., & Waliser, D. E. (2015). Detection of atmospheric rivers: Evaluation and application of an algorithm for global studies. *Journal of Geophysical Research: Atmospheres*, *120*(24), 12514–12535. https://doi.org/10.1002/2015JD024257Guan, B., & Waliser, D. E. (2019). Tracking Atmospheric Rivers Globally: Spatial Distributions and Temporal Evolution of Life Cycle Characteristics. *Journal of Geophysical Research: Atmospheres*, *124*(23), 12523–12552. https://doi.org/10.1029/2019JD031205Guan, B., Waliser, D. E., & Ralph, F.M. (2018). An intercomparison between reanalysis and dropsonde observations of the total water vapor transport in individual atmospheric rivers. *Journal of Hydrometeorology*, *19*(2), 321–337. https://doi.org/10.1175/JHM-D-17-0114.1Guo, Y., Shinoda, T., Guan, B., Waliser, D. E., & Chang, E. K. M. (2020). Statistical relationship between atmospheric rivers and extratropical cyclones and anticyclones. *Journal of Climate*, *33*(18), 7817–7834. https://doi.org/10.1175/JCLI-D-19-0126.1Hecht, C. W., & Cordeira, J. M. (2017). Characterising the influence of atmospheric river orientation and intensity on precipitation distributions over North Coastal California. *Geophysical Research Letters*, *44*(17), 9048–9058. https://doi.org/10.1002/2017GL074179Kingston, D. G., Lavers, D. A., & Hannah, D. M. (2016). Floods in the Southern Alps of New Zealand: the importance of atmospheric rivers. *Hydrological Processes*, *30*(26), 5063–5070. https://doi.org/10.1002/hyp.10982Lamjiri, M. A., Dettinger, M. D., Ralph, F. M., & Guan, B. (2017). Hourly storm characteristics along the U.S. West Coast: Role of atmospheric rivers in extreme precipitation. *Geophysical Research Letters*, *44*(13), 7020–7028. https://doi.org/10.1002/2017GL074193Lavers, D. A., Allan, R. P., Wood, E. F., Villarini, G., Brayshaw, D. J., & Wade, A. J. (2011). Winter floods in Britain are connected to atmospheric rivers. *Geophysical Research Letters*, *38*(23), 1–8. https://doi.org/10.1029/2011GL049783Lavers, D. A., & Villarini, G. (2013a). The nexus between atmospheric rivers and extreme precipitation across Europe. *Geophysical Research Letters*, *40*(12),

3259–3264. https://doi.org/10.1002/grl.50636Lavers, D. A., & Villarini, G. (2013b). Atmospheric Rivers and Flooding over the Central United States. *Journal of Climate*, *26*(20), 7829–7836. https://doi.org/10.1175/JCLI-D-13-00212.1Lavers, D. A., & Villarini, G. (2015). The contribution of atmospheric rivers to precipitation in Europe and the United States. *Journal of Hydrology*, *522*, 382–390. https://doi.org/10.1016/j.jhydrol.2014.12.010Lavers, D. A., Villarini, G., Allan, R. P., Wood, E. F., & Wade, A. J. (2012). The detection of atmospheric rivers in atmospheric reanalyses and their links to British winter floods and the large-scale climatic circulation. *Journal of Geophysical Research: Atmospheres*, *117*(D20), 1–13. https://doi.org/10.1029/2012JD018027Little, K., Kingston, D. G., Cullen, N. J., & Gibson, P. B. (2019). The Role of Atmospheric Rivers for Extreme Ablation and Snowfall Events in the Southern Alps of New Zealand. *Geophysical Research Letters*, *46*(5), 2761–2771. https://doi.org/10.1029/2018GL081669Liu, X., Ma, X., Chang, P., Jia, Y., Fu, D., Xu, G., Wu, L., Saravanan, R., & Patricola, C. M. (2021). Ocean fronts and eddies force atmospheric rivers and heavy precipitation in western North America. *Nature Communications*, *12*(1), 1–10. https://doi.org/10.1038/s41467-021-21504-wNayak, M. A., & Villarini, G. (2017). A long-term perspective of the hydroclimatological impacts of atmospheric rivers over the central United States. *Water Resources Research*, *53*(2), 1144–1166. https://doi.org/10.1002/2016WR019033Neiman, P. J., Ralph, F. M., Wick, G. A., Lundquist, J. D., & Dettinger, M. D. (2008). Meteorological Characteristics and Overland Precipitation Impacts of Atmospheric Rivers Affecting the West Coast of North America Based on Eight Years of SSM/I Satellite Observations. *Journal of Hydrometeorology*, *9*(1), 22–47. https://doi.org/10.1175/2007JHM855.1Neiman, P. J., Schick, L. J., Ralph, F. M., Hughes, M., & Wick, G. A. (2011). Flooding in Western Washington: The Connection to Atmospheric Rivers*. *Journal of Hydrometeorology*, *12*(6), 1337–1358. https://doi.org/10.1175/2011JHM1358.1Newell, R. E., Newell, N. E., Zhu, Y., & Scott, C. (1992). Tropospheric rivers? - A pilot study. *Geophysical Research Letters*, *19*(24), 2401–2404. https://doi.org/10.1029/92GL02916Newell, R. E., & Zhu, Y. (1994). Tropospheric rivers: A one-year record and a possible application to ice core data. *Geophysical Research Letters*, *21*(2), 113–116. https://doi.org/10.1029/93GL03113Paltan, H., Waliser, D., Lim, W. H., Guan, B., Yamazaki, D., Pant, R., & Dadson, S. (2017). Global Floods and Water Availability Driven by Atmospheric Rivers. *Geophysical Research Letters*, *44*(20), 10,387-10,395. https://doi.org/10.1002/2017GL074882Pan, M., & Lu, M. (2019). A Novel Atmospheric River Identification Algorithm. *Water Resources Research*, *55*(7), 6069–6087. https://doi.org/10.1029/2018WR024407Pfahl, S., & Wernli, H. (2012). Quantifying the Relevance of Cyclones for Precipitation Extremes. *Journal of Climate*, *25*(19), 6770–6780. https://doi.org/10.1175/JCLI-D-11-00705.1Porhemmat, R., Purdie, H., Zawar-Reza, P., Zammit, C., & Kerr, T. (2020). Moisture Transport during Large Snowfall Events in the New Zealand Southern Alps: The Role of Atmospheric Rivers. *Journal of Hydrometeorology*, *22*(2), 425–444. https://doi.org/10.1175/jhm-d-20-0044.1Prince, H.

D., Cullen, N. J., Gibson, P. B., Conway, J., & Kingston, D. G. (2021). A climatology of atmospheric rivers in New Zealand. *Journal of Climate*, *34*(11), 4383–4402. https://doi.org/10.1175/JCLI-D-20-0664.1Ralph, F. M., Coleman, T., Neiman, P. J., Zamora, R. J., & Dettinger, M. D. (2013). Observed Impacts of Duration and Seasonality of Atmospheric-River Landfalls on Soil Moisture and Runoff in Coastal Northern California. *Journal of Hydrometeorology*, *14*(2), 443–459. https://doi.org/10.1175/JHM-D-12-076.1Ralph, F. M., & Dettinger, M. D. (2012). Historical and National Perspectives on Extreme West Coast Precipitation Associated with Atmospheric Rivers during December 2010. *Bulletin of the American Meteorological Society*, *93*(6), 783–790. https://doi.org/10.1175/BAMS-D-11-00188.1Ralph, F. M., Rutz, J. J., Cordeira, J. M., Dettinger, M., Anderson, M., Reynolds, D., Schick, L. J., & Smallcomb, C. (2019). A scale to characterise the strength and impacts of atmospheric rivers. *Bulletin of the American Meteorological Society*, *100*(2), 269–289. https://doi.org/10.1175/BAMS-D-18-0023.1Ralph, F. M., Dettinger, M. D., Cairns, M. M., Galarneau, T. J., & Eylander, J. (2018). Defining "Atmospheric River": How the Glossary of Meteorology Helped Resolve a Debate. *Bulletin of the American Meteorological Society*, *99*(4), 837–839. https://doi.org/10.1175/BAMS-D-17-0157.1Ralph, F. M., Neiman, P. J., & Rotunno, R. (2005). Dropsonde Observations in Low-Level Jets over the Northeastern Pacific Ocean from CALJET-1998 and PACJET-2001: Mean Vertical-Profile and Atmospheric-River Characteristics. *Monthly Weather Review*, *133*(4), 889–910. https://doi.org/10.1175/MWR2896.1Ralph, F. M., Neiman, P. J., & Wick, G. A. (2004). Satellite and CALJET Aircraft Observations of Atmospheric Rivers over the Eastern North Pacific Ocean during the Winter of 1997/98. *Monthly Weather Review*, *132*(7), 1721–1745. https://doi.org/10.1175/1520-0493(2004)132<1721:SACAOO>2.0.CO;2Ralph, F. M., Neiman, P. J., Wick, G. A., Gutman, S. I., Dettinger, M. D., Cayan, D. R., & White, A. B. (2006). Flooding on California's Russian River: Role of atmospheric rivers. *Geophysical Research Letters*, *33*(13), L13801. https://doi.org/10.1029/2006GL026689Ralph, F. M., Wilson, A. M., Shulgina, T., Kawzenuk, B., Sellars, S., Rutz, J. J., Lamjiri, M. A., Barnes, E. A., Gershunov, A., Guan, B., Nardi, K. M., Osborne, T., & Wick, G. A. (2019). ARTMIP-early start comparison of atmospheric river detection tools: how many atmospheric rivers hit northern California's Russian River watershed? *Climate Dynamics*, *52*(7–8), 4973–4994. https://doi.org/10.1007/s00382-018-4427-5Reid, K. J., King, A. D., Lane, T. P., & Short, E. (2020). The Sensitivity of Atmospheric River Identification to Integrated Water Vapor Transport Threshold, Resolution, and Regridding Method. *Journal of Geophysical Research: Atmospheres*, *125*(20), 1–15. https://doi.org/10.1029/2020JD032897Reid, K. J., Rosier, S. M., Harrington, L. J., King, A. D., & Lane, T. P. (2021). Extreme rainfall in New Zealand and its association with Atmospheric Rivers. *Environmental Research Letters*, *16*(4). https://doi.org/10.1088/1748-9326/abeae0Saha, S., Moorthi, S., Pan, H.-L., Wu, X., Wang, J., Nadiga, S., Tripp, P., Kistler, R., Woollen, J., Behringer, D., Liu, H., Stokes, D., Grumbine, R., Gayno, G., Wang, J., Hou, Y.-T.,

Chuang, H., Juang, H.-M. H., Sela, J., … Goldberg, M. (2010). The NCEP Climate Forecast System Reanalysis. *Bulletin of the American Meteorological Society*, *91*(8), 1015–1058. https://doi.org/10.1175/2010BAMS3001.1Salinger, M. J. (1980). New Zealand Climate: I. Precipitation Patterns. *Monthly Weather Review*, *108*(11), 1892–1904. https://doi.org/10.1175/1520-0493(1980)108<1892:NZCIPP>2.0.CO;2Shields, C. A., Rutz, J. J., Leung, L.-Y., Ralph, F. M., Wehner, M., Kawzenuk, B., Lora, J. M., McClenny, E., Osborne, T., Payne, A. E., Ullrich, P., Gershunov, A., Goldenson, N., Guan, B., Qian, Y., Ramos, A. M., Sarangi, C., Sellars, S., Gorodetskaya, I., … Nguyen, P. (2018). Atmospheric River Tracking Method Intercomparison Project (ARTMIP): project goals and experimental design. *Geoscientific Model Development*, *11*(6), 2455–2474. https://doi.org/10.5194/gmd-11-2455-2018Shu, J., Shamseldin, A. Y., & Weller, E. (2021). The impact of atmospheric rivers on rainfall in New Zealand. *Scientific Reports*, *11*(1), 5869. https://doi.org/10.1038/s41598-021-85297-0Sinclair, M. R. (1994). An Objective Cyclone Climatology for the Southern Hemisphere. *Monthly Weather Review*, *122*(10), 2239–2256. https://doi.org/10.1175/1520-0493(1994)122<2239:AOCCFT>2.0.CO;2Sodemann, H., & Stohl, A. (2013). Moisture origin and meridional transport in atmospheric rivers and their association with multiple cyclones. *Monthly Weather Review*, *141*(8), 2850–2868. https://doi.org/10.1175/MWR-D-12-00256.1Tait, A. B., & Fitzharris, B. B. (1998). Relationships between New Zealand rainfall and south-west Pacific pressure patterns. *International Journal of Climatology*, *18*(4), 407–424. https://doi.org/10.1002/(SICI)1097-0088(19980330)18:4<407::AID-JOC256>3.0.CO;2-SViale, M., Valenzuela, R., Garreaud, R. D., & Ralph, F. M. (2018). Impacts of Atmospheric Rivers on Precipitation in Southern South America. *Journal of Hydrometeorology*, *19*(10), 1671–1687. https://doi.org/10.1175/JHM-D-18-0006.1Waliser, D., & Guan, B. (2017). Extreme winds and precipitation during landfall of atmospheric rivers. *Nature Geoscience*, *10*(3), 179–183. https://doi.org/10.1038/ngeo2894Watts, I. E. M. (1947). THE RELATIONS OF NEW ZEALAND WEATHER AND CLIMATE: AN ANALYSIS OF THE WESTERLIES. *New Zealand Geographer*, *3*(2), 115–129. https://doi.org/10.1111/j.1745-7939.1947.tb01458.xZhang, Z., Ralph, F. M., & Zheng, M. (2019). The Relationship Between Extratropical Cyclone Strength and Atmospheric River Intensity and Position. *Geophysical Research Letters*, *46*(3), 1814–1823. https://doi.org/10.1029/2018GL079071Zhou, Y., & Kim, H. (2019). Impact of Distinct Origin Locations on the Life Cycles of Landfalling Atmospheric Rivers Over the U.S. West Coast. *Journal of Geophysical Research: Atmospheres*, *124*(22), 11897–11909. https://doi.org/10.1029/2019JD031218Zhou, Y., Kim, H., & Guan, B. (2018). Life Cycle of Atmospheric Rivers: Identification and Climatological Characteristics. *Journal of Geophysical Research: Atmospheres*, *123*(22), 12,715-12,725. https://doi.org/10.1029/2018JD029180Zhu, Y., & Newell, R. E. (1994). Atmospheric rivers and bombs. *Geophysical Research Letters*, *21*(18), 1999–2002. https://doi.org/10.1029/94GL01710Zhu, Y., & Newell, R. E. (1998). A Proposed Algorithm for Moisture Fluxes from Atmospheric Rivers.

Monthly Weather Review, *126*(3), 725–735. https://doi.org/10.1175/1520-0493(1998)126<0725:APAFMF>2.0.CO;2